J. Non-Newtonian Fluid Mech. 166 (2011) 145–151

Contents lists available at ScienceDirect

Journal of Non-Newtonian Fluid Mechanics

journal homepage: www.elsevier.com/locate/jnnfm

Bingham fluid simulation with the incompressible lattice Boltzmann model

G.H. Tang*, S.B. Wang, P.X. Ye, W.Q. Tao

State Key Lab of Multiphase Flow, School of Energy and Power Engineering, Xi'an Jiaotong University, 28, Xianning West Road, Xi'an 710049, China

ARTICLE INFO

Article history:
Received 2 September 2010
Received in revised form 24 October 2010
Accepted 4 November 2010

Keywords:
Non-Newtonian fluid
Lattice Boltzmann method
Bingham fluid
Yield stress
Cavity flow
Expansion flow

ABSTRACT

The Bingham fluid flow is numerically studied using the lattice Boltzmann method by incorporating the Papanastasiou exponential modification approach. The He–Luo incompressible lattice Boltzmann model is employed to avoid numerical instability usually encountered in non-Newtonian fluid simulations due to a strong non-linear relationship between the shear rate tensor and the rate-of-strain tensor. First, the value of the regularization parameter in Bingham fluid mimicking is analyzed and a method to determine the value is proposed. Then, the model is validated by pressure-driven planar channel flow and planar sudden expansion flow. The velocity profiles for the pressure-driven planar channel flow are in good agreement with analytical solutions. The calculated reattachment lengths for a 2:1 planar sudden expansion flow also agree well with the available data. Finally, the Bingham flow over a cavity is studied, and the streamlines and yielded/unyielded regions are discussed.

1. Introduction

The studies of non-Newtonian fluids and the flow behaviors are of high interest to a broad range of disciplines in both science and technology, including hydrology, geophysics, materials, food, and biology. A plastic non-Newtonian fluid such as slurry, paste, paint, and margarine, only flows above a certain level of stress, called yield stress, while it exhibits little or no deformation below this yield stress. These materials are usually called Bingham plastics or Bingham fluids [1]. In many cases of interest, due to the limitation of analytical solutions it is highly desirable to find efficient numerical methods for such non-Newtonian flows under complex rheology properties and complicated bounded geometries. Though significant progress has been made in developing numerical approaches for such viscoplastic flows in various geometries, most of these schemes are based on traditional finite difference or finite element discretization in which a set of appropriate partial differential equations are discretized and solved [2–7].

The recently developed lattice Boltzmann method (LBM), due to its inherent vantages like simple implementation, high parallelizability and great convenience of handling complicated geometries and boundary conditions, has been successfully developed to study complex transport phenomena and model complex physics [8,9] which are usually hardly accessible to traditional macroscopic approaches. The kinetic essence of the LBM makes it also capable of calculating the local components of the stress tensor directly. The lattice Boltzmann models have been set up for non-Newtonian flow systems in the literature recently [10–20] by adjusting the relaxation time (and hence the viscosity) to the local shear rate. Thereinto, Wang and Ho [17] proposed a lattice Boltzmann model particularly for Bingham fluid by incorporating the effect of local shear rate into the lattice equilibrium distribution function, and a planar sudden expansion flow was examined. Vikhansky [18] proposed a novel and efficient version of the LBM for non-Newtonian flow simulation and the collisions are treated implicitly, i.e., the collision term is chosen such that the stress and strain rate tensors satisfy the constitutive equation after the collision. The method does not need any regularization and the Bingham flow was examined in his work. However, some velocity derivatives are introduced into the density equilibrium distribution function in Ref. [17], while in Ref. [18], a non-linear equation linking stress intensity with shear rate has to be solved at each node and each time step additionally. In this wok, still basing on the traditional lattice Boltzmann framework, we employ a fairly simple lattice Boltzmann scheme, the He–Luo incompressible model [21], with incorporation of the popular Papanastasiou exponential modification approach [22], to simulate the Bingham fluid flow.

2. Numerical methods

2.1. The Papanastasiou approach for Bingham fluid

In order to model the stress-deformation behavior of Bingham fluids, the ideal Bingham constitutive equations have been pro-

* Corresponding author.
E-mail address: ghtang@mail.xjtu.edu.cn (G.H. Tang).

0377-0257/$ – see front matter © 2010 Elsevier B.V. All rights reserved.
doi:10.1016/j.jnnfm.2010.11.005

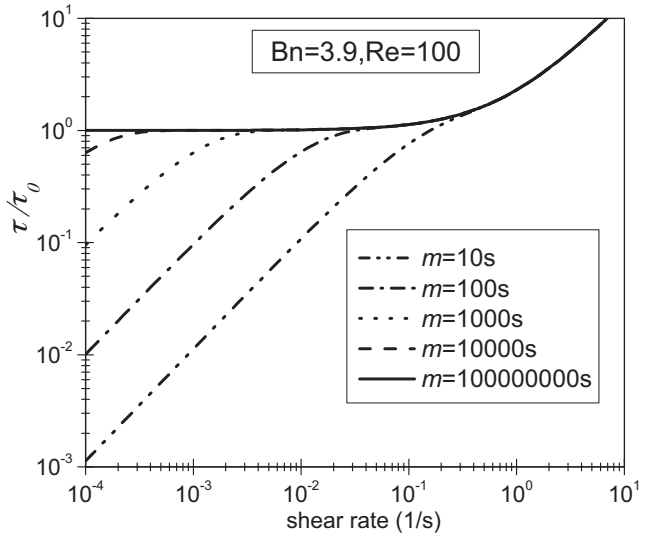

Fig. 1. The dimensionless shear stress against shear rate $\dot{\gamma}$ according to the modified Bingham constitutive equation (2) for several values of the exponent m.

posed as [23]

$$\tau = \tau_0 + \eta_p \dot{\gamma} \quad \text{if} \quad |\tau| > \tau_0, \tag{1a}$$

$$\dot{\gamma} = 0 \quad \text{if} \quad |\tau| \le \tau_0, \tag{1b}$$

where τ is the shear stress tensor, τ_0 is the yield stress, η_p is a constant plastic viscosity, and $\dot{\gamma}$ is the shear rate tensor. From these constitutive relations, it is known that when the magnitude of shear stress τ falls below τ_0, the material becomes a solid structure (unyielded). In order to avoid the inherent attribute of discontinuity in the viscoplastic model, Papanastasiou [22] proposed a modified equation that makes the shear stress vary continuously with the shear rate. This called regularization method makes the equation valid for both yielded and unyielded areas. With Papanastasiou exponential modification, the Bingham model becomes

$$\tau = \tau_0[1 - \exp(m\dot{\gamma})] + \eta_p \dot{\gamma}, \tag{2}$$

where m is the regularization parameter or the stress growth exponent, which controls the exponential growth of the stress. Ideal Bingham fluid can be mimicked for a large enough regularization parameter m to guarantee large apparent viscosity at vanishing rates of strain. Then from Eq. (2) the apparent viscosity of the Bingham fluid can be expressed as

$$\eta = \frac{\tau}{\dot{\gamma}} = \eta_p + \frac{\tau_0}{\dot{\gamma}}[1 - \exp(-m\dot{\gamma})], \tag{3}$$

where $\dot{\gamma}$ is the second invariant of the rate-of-strain tensor given by $\dot{\gamma} = \sqrt{2S_{\alpha\beta}S_{\alpha\beta}}$ and $S_{\alpha\beta}$ is defined as

$$S_{\alpha\beta} = \frac{1}{2}\left(\frac{\partial u_\alpha}{\partial x_\beta} + \frac{\partial u_\beta}{\partial x_\alpha}\right). \tag{4}$$

Expressions mentioned above enable the shear stress to change continuously with the variation of shear rate.

To examine the effect of the value of exponent m on the approximation degree to ideal Bingham fluid, we present the shear stress against shear rate according to the modified Bingham constitutive equation (2) for several values of the exponent m. As shown in Fig. 1, the dimensionless shear stress τ/τ_0 approaches the ideal Bingham fluid (the solid line in the figure) as the value of m increases, which indicates that this equation can mimic the ideal Bingham fluid accurately for large enough m. However, in practical simulation, the value of m cannot be too large since it will result in numerical instability [24]. An intermediate value of m is usually chosen in the literature like $m = 1000$ s [5,17,24]. However, under the conditions of a fixed Reynolds number and exponent m, the approximation degree to the ideal Bingham fluid deviates obviously if we change Bingham number during the simulation as shown in Fig. 2, in which the apparent viscosity calculated by Eq. (3) varies against the shear rate for different Bingham numbers at fixed Re = 100 and $m = 1000$ s. We can see that when Bingham number is large, the apparent viscosity at lower shear rate is much larger than the viscosity at larger shear rate and hence the Bingham fluid can be mimicked very well. On the contrary, when Bingham number is small, the exhibited apparent viscosity difference between the lower shear rate and the larger shear rate is so small that the Bingham fluid is difficult to mimic. Therefore a much larger value of exponent m is suggested for this situation as shown in Fig. 3. From Fig. 3 we can see that the Bingham fluid can be mimicked well by adjusting $m = 10{,}000$–$100{,}000$ s at Re = 100 and a small Bingham number Bn = 0.01. Here the Reynolds number and Bingham number are defined as, respectively,

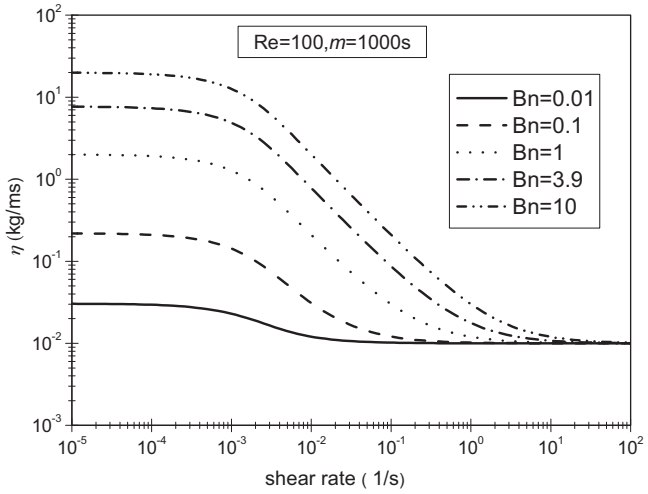

Fig. 2. The Bingham apparent viscosity against shear rate $\dot{\gamma}$ for different Bingham numbers at Re = 100 and $m = 1000$ s.

$$Re = \frac{\rho \bar{u} H}{2\eta_p}, \tag{5}$$

$$\mathrm{Bn} = \frac{\tau_0 H}{\eta_p \bar{u}}, \tag{6}$$

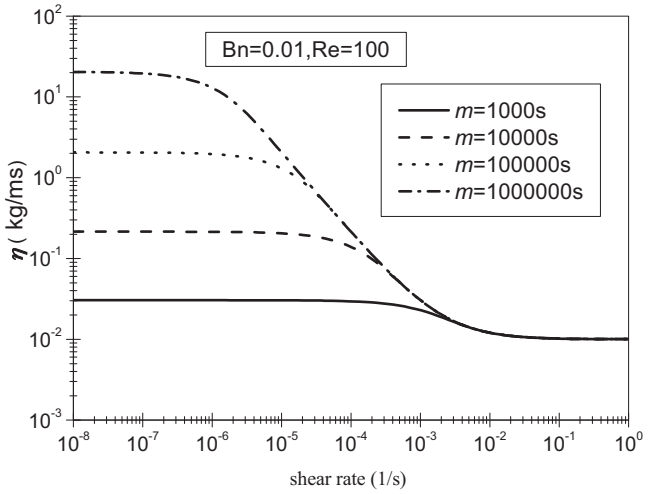

Fig. 3. The Bingham apparent viscosity against shear rate $\dot{\gamma}$ for different values of exponent m at a small Bingham number Bn = 0.01 and Re = 100.

where H is the characteristic length, and $\bar{u}$ is the average streamwise velocity of the Bingham fluid flow. In practical simulations, we can decide the value of exponent m by keeping the apparent viscosity ratio of lower shear rate to higher shear rate within an appropriate range. If defining this apparent viscosity ratio as M, we can obtain the following expression approximately from Eq. (2):

$$m = M\frac{\eta_p}{\tau_0}. \tag{7}$$

With definitions for Reynolds number and Bingham number in Eqs. (5) and (6), respectively, Eq. (7) in terms of M can be rewritten as

$$m = \frac{M}{2}\frac{\rho H^2}{\eta_p \mathrm{Bn}\,\mathrm{Re}}. \tag{8}$$

Hence we can determine the value of m conveniently in the specified simulation. In our experiences, the value of ratio M can usually be chosen between 10 and 50 in the simulation.

2.2. The lattice Boltzmann model

In this subsection, the lattice Boltzmann equation for Bingham fluids is established. The LBM can be looked as a simplified utilization of the Boltzmann equation on a discrete lattice with a series of discrete velocity distribution functions. The evolution equation with a single relaxation time of BGK approximation can be expressed as

$$f_i(\mathbf{r}+\mathbf{c}_i\delta_t, t+\delta_t) - f_i(\mathbf{r}, t) = -\frac{1}{\tau}(f_i(\mathbf{r}, t) - f_i^{eq}(\mathbf{r}, t)), \tag{9}$$

where f_i is the particle distribution function in the i direction, $f_i^{eq}(\mathbf{r}, t)$ is the equilibrium distribution function, τ is the relaxation time, $\mathbf{r}$ is the position vector, and $\mathbf{c}_i$ is the lattice velocity along the i direction. For a two-dimensional D2Q9 square lattice [8], we have $\mathbf{c}_0 = 0$, $\mathbf{c}_i = (\cos[(i-1)\pi/2], \sin[(i-1)\pi/2])c$ for $i = 1, 2, 3, 4$ and $\mathbf{c}_i = (\cos[(i-5)\pi/2+\pi/4], \sin[(i-5)\pi/2+\pi/4])\sqrt{2}c$ for $i = 5, 6, 7, 8$, where $c = \delta_x/\delta_t$ is the particle streaming speed (δ_x and δ_t are the lattice spacing and time step, respectively).

It is known that the shear stress tensor exhibits a strong non-linear relationship with the shear rate tensor for most non-Newtonian fluid flows. During the simulation of non-Newtonian fluids using the standard lattice BGK model which is of nearly incompressible limit under low Mach number, the local density is significantly affected by the radical variation of the local non-Newtonian viscosity. And therefore the numerical stability is often difficult to attain. Wang and Ho [17] particularly incorporated the effect of local shear rate into the lattice equilibrium distribution function to overcome this numerical instability. Vikhansky [18] proposed a novel and efficient version of the LBM for non-Newtonian flow simulation by using the implicit collisions and any regularization is not needed in his model. In this work we employ the He–Luo incompressible lattice Boltzmann model, in which pressure p is used as an independent dynamic variable instead of the mass density ρ. It could completely eliminate the compressible effect of the standard lattice Boltzmann models by neglecting the terms of higher order Mach number. In this model, the pressure distribution functions are used instead of the density distribution functions as:

$$p_i^{eq} \equiv c_s^2 f_i^{eq} = \omega_i \left\{ p + p_0 \left[3\frac{(\mathbf{c}_i\cdot\mathbf{u})}{c^2} + \frac{9}{2}\frac{(\mathbf{c}_i\cdot\mathbf{u})^2}{c^4} - \frac{3}{2}\frac{\mathbf{u}^2}{c^2} \right] \right\}, \tag{10}$$

where $p = c_s^2\rho$ is the pressure at a specified position with the sound speed $c_s = c/\sqrt{3}$ for the D2Q9 model, p_0 is the constant pressure with $p_0 = c_s^2\rho_0$, and the weight factor $\omega_0 = 4/9$, $\omega_1 = \omega_2 = \omega_3 = \omega_4 = 1/9$, and $\omega_5 = \omega_6 = \omega_7 = \omega_8 = 1/36$. Accordingly,

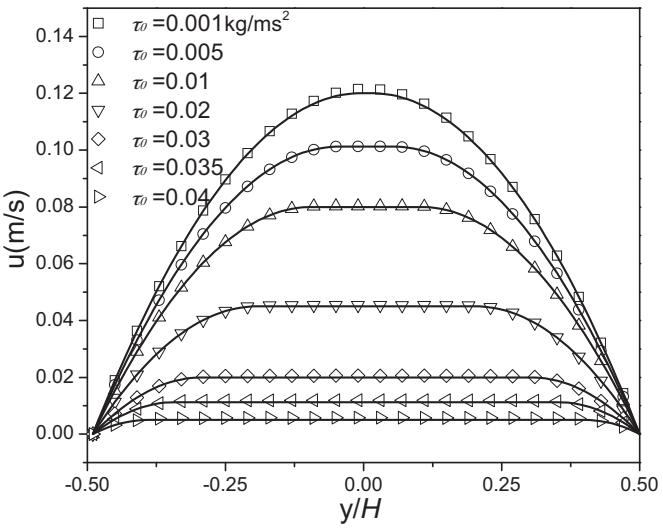

Fig. 4. Streamwise velocity profiles for the pressure-driven planar channel flow of Bingham fluid. Symbols are the present LBM results and lines are the analytical solutions in Ref. [26].

the evolution equation of the LBM system, Eq. (9), becomes:

$$p_i(\mathbf{r}+\mathbf{c}_i\delta_t, t+\delta_t) - p_i(\mathbf{r}, t) = -\frac{1}{\tau}[p_i(\mathbf{r}, t) - p_i^{eq}(\mathbf{r}, t)], \tag{11}$$

where the pressure p and velocity vector $\mathbf{u}$ are given by

$$p = \sum_i p_i, \qquad p_0\boldsymbol{u} = \sum_i \mathbf{c}_i p_i. \tag{12}$$

Through the Chapman-Enskog procedure, the continuum incompressible Navier–Stokes equations accurate to the order of Mach number $O(Ma^2)$ in continuity equation and $O(Ma^3)$ in momentum equation can be derived from the incompressible lattice Boltzmann model with rigor (see Ref. [21] for details):

$$\nabla\cdot\mathbf{u} = 0 + O(Ma^2), \tag{13a}$$

$$\rho_0\frac{\partial\mathbf{u}}{\partial t} + \rho_0\mathbf{u}\cdot\nabla\mathbf{u} = -\nabla p + \eta\nabla^2\mathbf{u} + O(Ma^3). \tag{13b}$$

The local viscosity is related with the local relaxation time in the lattice Boltzmann evolution Eq. (11) by

$$\tau = 3\frac{\eta(\dot{\gamma})}{\rho_0}\frac{\delta_t^2}{\delta_x^2} + 0.5\delta_t. \tag{14}$$

With the combination of Eqs. (3) and (14) the lattice Boltzmann model for Bingham fluid is constructed.

3. Results and discussion

In order to examine the performance of the present model, computation of the planar Poiseuille flow of Bingham fluids driven by a constant pressure difference is conducted first. The calculation is carried out on a domain of 100×500 uniform D2Q9 lattices. The characteristic length of the parallel channel height is $H = 0.1$ m, pressure gradient of 1.0 Pa/m is applied as a force term, viscosity is set to be $\eta_p = 0.01$ kg/ms, and yield stress τ_0 varies from 0.001 to 0.04 kg/ms^2. The periodic boundary conditions for the channel inlet and outlet, and the no-slip wall boundary conditions proposed by Zou and He [25] are employed. Fig. 4 shows that the velocity profiles of the present LBM are in good agreement with the analytical solutions [26] within the shown yield stress range and the velocity increases as the yield stress decreases. As the yield stress increases, the velocity profile changes from a parabola to a flat plateau occur-

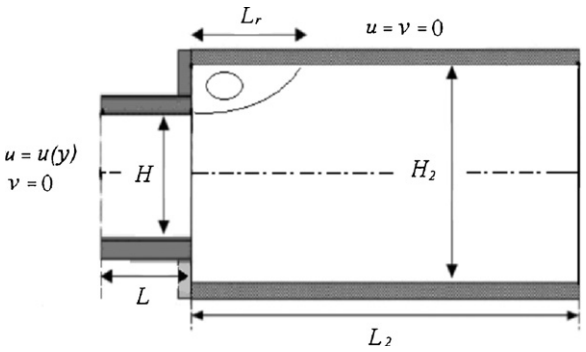

Fig. 5. Schematic of a planar expansion flow.

ring in the channel center zone, which represents the unyielded material.

Secondly, a planar sudden expansion flow with a 2:1 expansion geometry schematic in Fig. 5 is examined. The whole domain is simulated regardless of the symmetry geometry. In Bingham fluid flows, it is also convenient to present the results using a dimensionless yield stress τ_0^*,

$$\tau_0^* = \frac{\tau_0 H}{2\eta_p \bar{u}_N}. \tag{15}$$

Here the characteristic length H in Eqs. (5), (6) and (15) is the height of channel entry section as schematic in Fig. 5, and the velocity $\bar{u}_N$ is defined as the average streamwise velocity of a corresponding Newtonian liquid with viscosity η_p at the same pressure gradient. The characteristic velocity $\bar{u}$ in Eqs. (5) and (6) is the average streamwise velocity of the Bingham fluid at the channel inlet. The Newtonian fluid recovers when $\tau_0^* = \mathrm{Bn} = 0$. Regarding the boundary conditions, the inlet velocity profile is fixed by assuming a fully developed channel flow for a Bingham fluid and the analytical solution is used. The pressure boundary condition with $p = 0$ is applied at the channel outlet and the no-slip boundary condition at the solid walls. The no-slip wall boundary condition and the pressure boundary condition by Zou and He [25] are used.

The progressive growth of the unyielded zone for Bingham flow in a 2:1 planar sudden expansion channel is shown in Figs. 6 and 7, where green color (light color) represents the yielded region and red color (deep color) for the unyielded region. In Fig. 6 the length of channel entry section is set to be $L = 2H$ and the length of channel expansion section $L_2 = 4H$, while in Fig. 7 a longer expansion length $L_2 = 6H$ is set to capture some phenomena occurring at high Reynolds numbers. After grid-independence test 100 uniform meshes is used for the scale of channel entry height H. Fig. 6 shows that the material is yielded along the channel wall owing to higher shear stress under fixed Re = 1 and Bingham number increasing from 3.9 to 3519. We can see that the unyielded zone is larger in the channel expansion section than in the entry section owing to the lower flow velocity (hence shear stress level) in the expansion section. In addition, the material remains unyielded in the dead spaces near the expansion corners due to the recirculation flow. With the Bingham number increasing, the unyielded zone increases both in the entry section and expansion section, and the solid region in the expansion section extends further to the expansion entrance. As the Bingham number reaches very high, the material remains yielded only in the high-gradient areas of the shear stress near the wall and the expansion entrance. With regard to fixed Bn = 3.9 in Fig. 7, increasing Reynolds number indicates that more material turns into flow motion. The material remains unyielded dead space around the expansion corners owing to the existence of vortex and recirculation of flow. The unyielded zone around the expansion corners grows larger as the recirculation zone increases

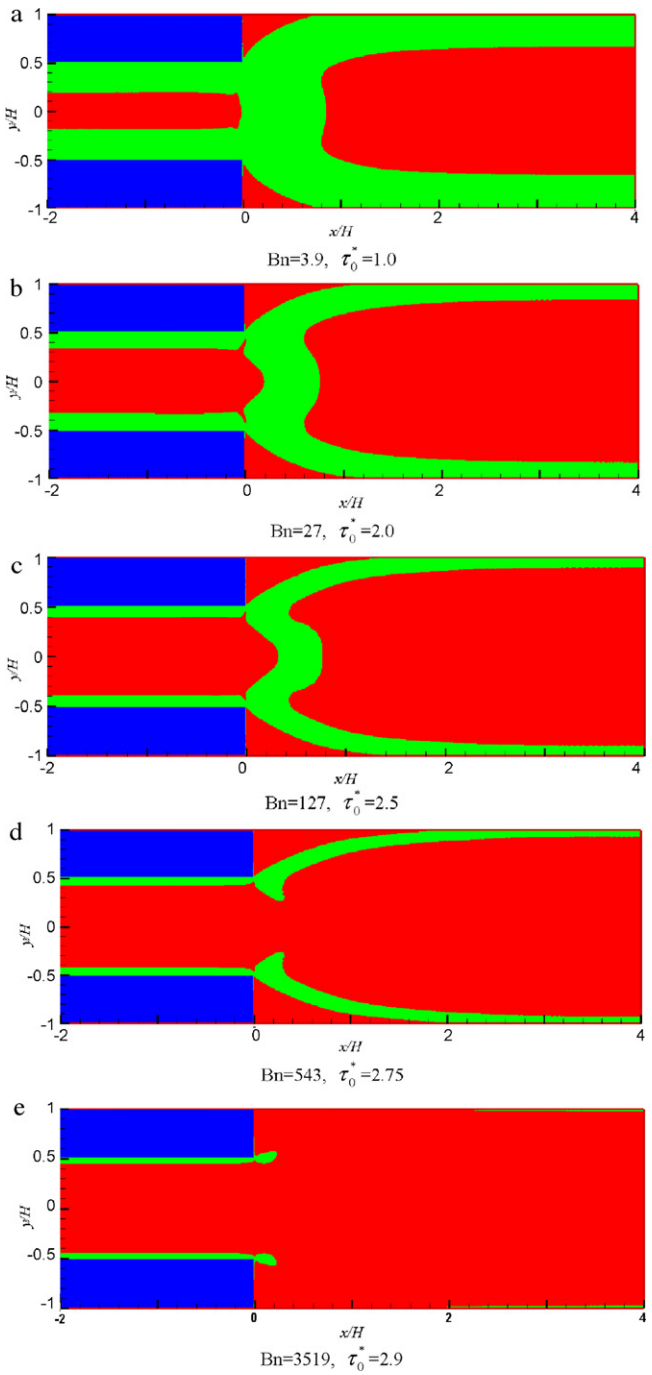

Fig. 6. The yielded/unyielded regions for Bn = 3.9, 27, 127, 543, and 3519 in a 2:1 planar sudden expansion flow (Re = 1).

at larger Reynolds numbers. Strictly speaking, no vortex activity occurs inside the unyielded regions since there is no deformation produces for the unyielded [5]. However, the using Papanastasiou exponential modification makes the Bingham model valid in all areas, both yielded and unyielded (for interpretation of the references to color in this sentence, the reader is referred to the web version of the article).

To compare the present LBM results with the available data quantitatively for the verification of flow dynamics in expansions, the dimensionless vortex length is calculated which is defined as the ratio of the reattachment length to the height of channel expansion section, L_r/H_2.

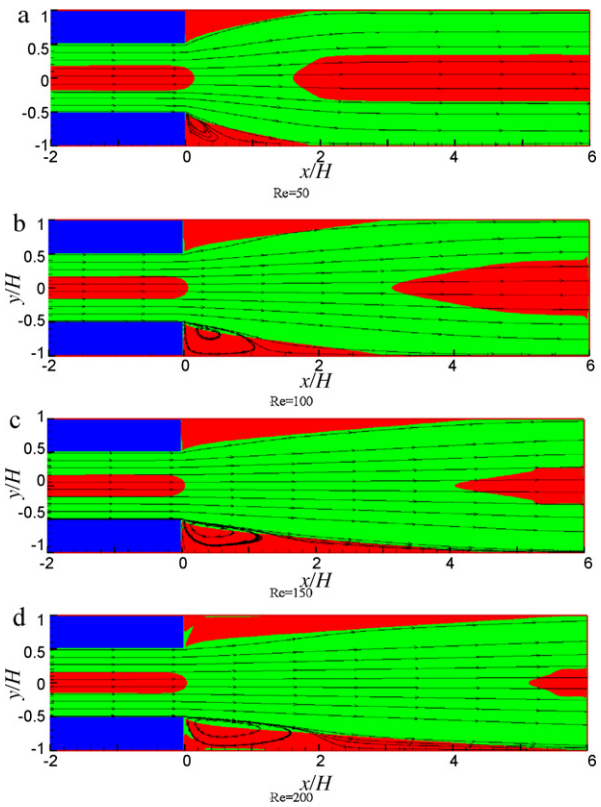

Fig. 7. The influences of Reynolds number in a 2:1 planar sudden expansion flow (Bn = 3.9).

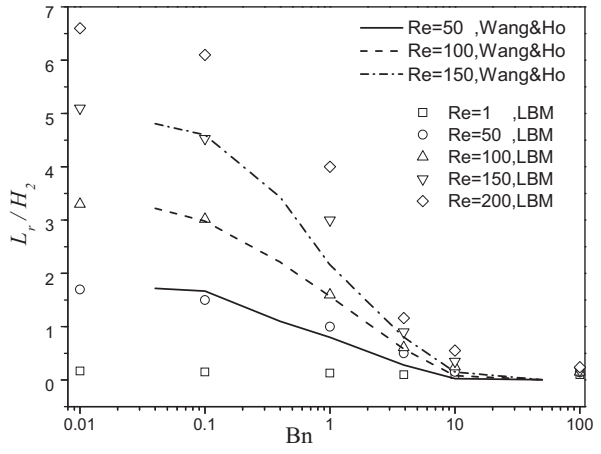

Fig. 8. Reattachment length against Bingham number for Bingham fluids flowing in a 2:1 planar sudden expansion at various Reynolds numbers.

Fig. 8 shows the dimensionless reattachment length as a function of Bn and Re in the 2:1 planar sudden expansion channel, in which the present LBM results (the symbols) are compared with the data by Wang and Ho (the lines) [17]. We can clearly see that the reattachment length increases with the increase in Reynolds number or the decrease in Bingham number. The results of the present LBM agree well with those in the reference. Compared to the data by Wang and Ho [17], wider ranges of Bingham number and Reynolds number are performed by using the He–Luo incompressible lattice Boltzmann model. This shows that the incompressible lattice Boltzmann model is a fairly stable and efficient scheme for Bingham fluid simulation.

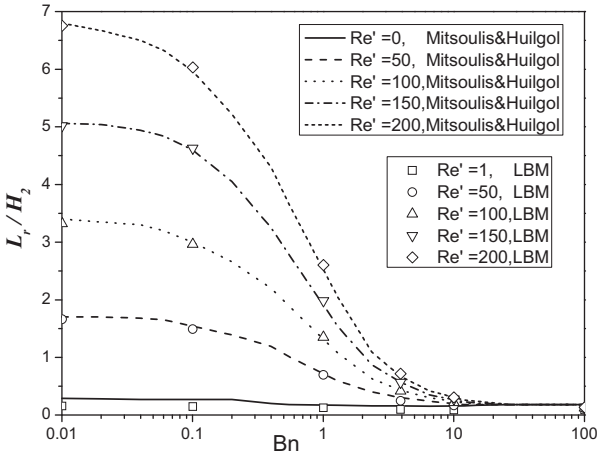

Fig. 9. Reattachment length against Bingham number for Bingham fluids flowing in a 2:1 planar sudden expansion at various Reynolds numbers. The Reynolds number is defined here as $\mathrm{Re}' = \rho \bar{u}_N H / 2\eta_p$ to compare with the data by Mitsoulis and Huilgol [5].

Mitsoulis and Huilgol [5] also presented detailed results for Bingham flow in a 2:1 sudden expansion channel by using the finite element method. However, a slightly different Reynolds number is defined as $\mathrm{Re}' = \rho \bar{u}_N H / 2\eta_p$, where Newtonian fluid velocity $\bar{u}_N$ is used as the characteristic velocity for Reynolds number. According to this definition, we perform the simulation again and the calculated dimensionless reattachment length is presented in Fig. 9, where $\mathrm{Re}' = 0$ in the reference represents the creeping flow. We can see that the present LBM results are also in good agreement with the data by the finite element method. Generally speaking, the computation effort for simple geometry simulation by the LBM is slightly more intensive compared to the traditional discretization approaches such as the finite element method [9]. However, the LBM is of high efficiency especially for complicated geometries and parallel computation. On the other hand, compared to the LBM models by incorporating some velocity derivatives into the equilibrium distribution function, the present approach is more efficient in computation time. Note that recently similar expansion flow for complex fluid was also investigated with the coarse-grained molecular dynamics simulation to reveal more microscope details [27].

Thirdly, a Bingham flow over a cavity schematic in Fig. 10 is simulated using the present LBM. During the simulation, the Reynolds number is defined as $Re = \rho \bar{u} H / 2\eta_p$ and fixed at Re = 1, and the Bingham number varies in the range of Bn = 1–1000. The boundary treatments at the channel inlet, outlet and solid walls are adopted as same as the above-studied sudden expansion flow. The number of 100 uniform meshes is employed for the scale of cavity height H. The streamlines and yielded/unyielded regions are presented in Fig. 11. From the figure we can see that the unyielded region in the channel grows larger and larger as the Bingham number increases. At Bn = 100, the unyielded region nearly fills the entire channel

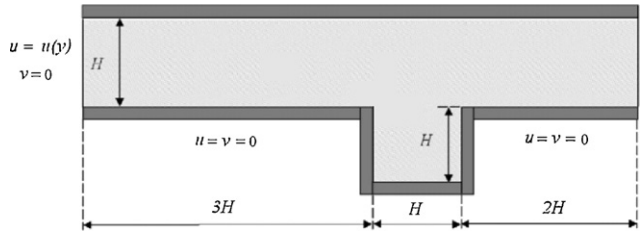

Fig. 10. Schematic of a flow over a square cavity.

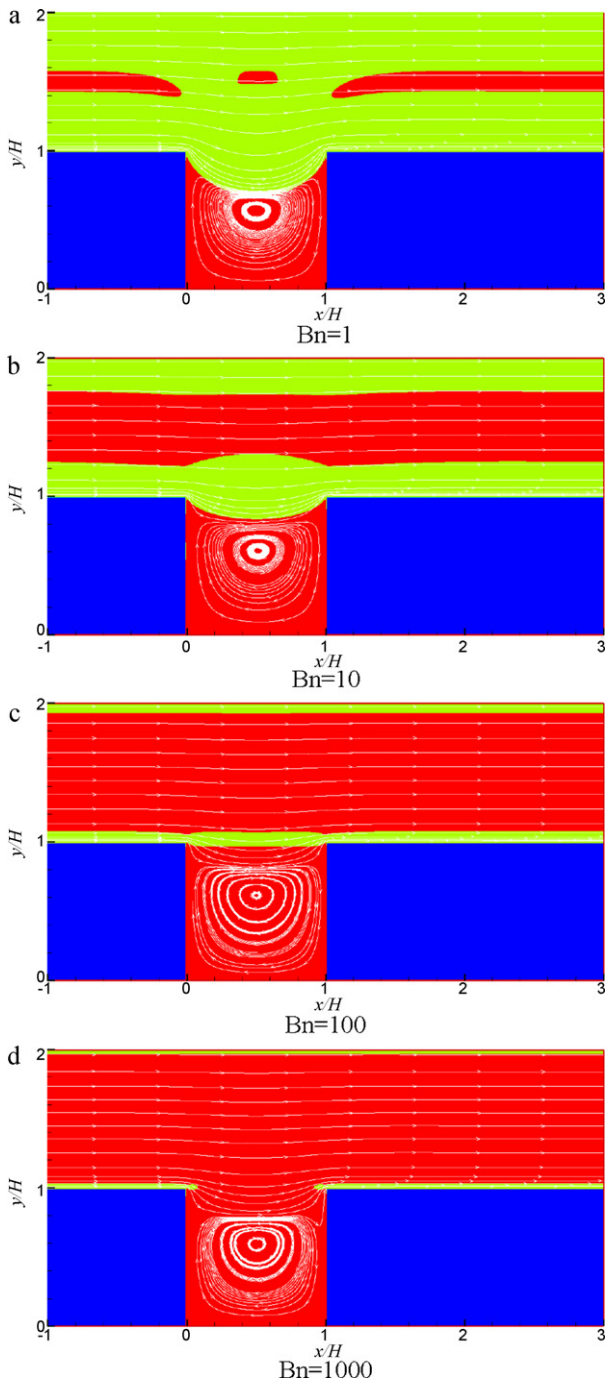

Fig. 11. Streamlines and yielded/unyielded regions for Bn = 1, 10, 100, and 1000 in Bingham fluid flow over a cavity (Re = 1).

except the yielded zone near the wall with high shear stress. For the material in the cavity, the yielded zone moves away from the cavity as the Bingham number increases. Most of the yielded region disappears from the cavity at Bn = 100. When the Bingham number reaches Bn = 1000, the yielded region disappears totally from the cavity and the unyielded region fills completely both the channel and the cavity, only leaving very thin boundary yielded layers adjacent to the wall. Regarding the streamline, it bends inside the cavity, indicating the presence of recirculation, and separates the mainstream in the channel from the secondary flow in the cavity. The vortex center of the secondary flow situates along the vertical centerline of the cavity and it moves upward slightly with the increasing Bingham number. The simulated results are in consistence with the study in Ref. [6].

An increase in numerical stability of the present model can be attributed to the followings. First, as stated in Ref. [21], in deriving the incompressible Navier–Stokes equations from the incompressible lattice Boltzmann model, an approximation is made to neglect the terms of higher order than the convection term of order March number, $O(Ma^2)$, in particular, the divergent term (compressibility). During the non-Newtonian simulation using the standard compressible lattice BGK model, we found that local density is significantly affected by the radical variation of the local viscosity. The cancel of density fluctuation makes the present scheme relatively stable and efficient. Secondly, we can keep the local relaxation time within an appropriate range by both adjusting the regularization parameter m with Eq. (8) and the lattice discrete velocity c to improve the numerical stability.

4. Conclusions

In this paper, by incorporating the Papanastasiou exponential modification, the He–Luo incompressible lattice Boltzmann model has been developed to simulate the Bingham flow. The numerical stability is improved attributed to the pressure-based distribution instead of density-based distribution in the lattice Boltzmann method. The effect of the regularization parameter m on the simulation of Bingham fluid was analyzed. By controlling the ratio of apparent viscosity at lower shear rate to higher shear rate, a method was proposed to determine the value of m and thus improve the numerical stability as well. The pressure-driven planar channel flow was validated with the present LBM and the computed velocity profiles are in good agreement with the analytical solutions. The 2:1 planar sudden expansion flow was studied over wide ranges of Reynolds number from 1 to 200 and Bingham number from 0 to 3500. The influences of both Reynolds number and Bingham number on the yielded/unyielded regions' growth and the reattachment length were discussed. The reattachment length increases with the increase in Reynolds number or the decrease in Bingham number. The present LBM results for the reattachment length agree well with the available data. The Bingham flow over a cavity was also studied and the influences of Bingham number on the streamlines and the yielded/unyielded regions were discussed. The unyielded region grows larger and larger as the Bingham number increases and the vortex center of the secondary flow in the cavity moves upward slightly with the increasing Bingham number. The present study shows that the He–Luo incompressible lattice Boltzmann model is of potential for simulating complex non-Newtonian fluid flow like Bingham fluid in which the shear stress tensor exhibits a strong non-linear relationship with the shear rate tensor.

Acknowledgments

This work was supported by the National Natural Science Foundation of China (No. 50776067), the Major State Basic Research and Development Program of China (No. 2011CB710702), and the Program for New Century Excellent Talents in University of China (No. NCET-07-0676).

References

[1] E.C. Bingham, Fluidity and Plasticity, McGraw-Hill, New York, 1922.
[2] P.S. Scott, F. Mirza, J. Vlachopoulos, Finite-element simulation of laminar viscoplastic flows with regions of recirculation, J. Rheol. 32 (1988) 387.
[3] S.S. Abdali, E. Mitsoulis, N.C. Markatos, Entry and exit flows of Bingham fluids, J. Rheol. 36 (1992) 389.
[4] E. Mitsoulis, S.S. Abdali, N.C. Markatos, Flow simulation of Herschel–Bulkley fluids through extrusion dies, Can. J. Chem. Eng. 71 (1993) 147.
[5] E. Mitsoulis, R.R. Huilgol, Entry flows of Bingham plastics in expansions, J. Non-Newtonian Fluid Mech. 122 (2004) 45.

[6] E. Mitsoulis, S. Marangoudakis, M. Spyratos, Th. Zisis, N.A. Malamataris, Pressure-driven flows of Bingham plastics over a square cavity, ASME J. Fluids Eng. 128 (2006) 993.
[7] G.R. Burgos, A.N. Alexandrou, Flow development of Herschel–Bulkley fluids in a sudden three-dimensional square expansion, J. Rheol. 43 (1999) 485.
[8] Y.H. Qian, D. d'Humieres, P. Lallemand, Lattice BGK models for Navier–Stokes equation, Europhys. Lett. 17 (1992) 479.
[9] S. Succi, Lattice Boltzmann Equation for Fluid Dynamics and Beyond, Clarendon Press, Oxford, 2001.
[10] E. Aharonov, D.H. Rothman, Non-Newotonian flow (through Porous media): a lattice Boltzmann method, Geophys. Res. Lett. 20 (1993) 679.
[11] E.S. Boek, J. Chiny, P.V. Coveney, Lattice Boltzmann simulations of the flow of non-Newtonian fluids in porous media, Int. J. Mod. Phys. B 17 (2003) 99.
[12] S. Gabbanelli, G. Drazer, J. Koplik, Lattice Boltzmann method for non-Newtonian (power-law) fluids, Phys. Rev. E 72 (2005) 046312.
[13] J. Boyd, J. Buick, S. Green, A second-order accurate lattice Boltzmann non-Newtonian flow model, J. Phys. A 39 (2006) 1424.
[14] S.P. Sullivan, L.F. Gladden, M.L. Johns, Simulation of power-law fluid flow through porous media using lattice Boltzmann techniques, J. Non-Newtonian Fluid Mech. 133 (2006) 91.
[15] J. Boyd, J. Buick, S. Green, Analysis of the Casson and Carreau-Yasuda non-Newtonian blood models in steady and oscillatory flows using the lattice Boltzmann method, Phys. Fluids 19 (2007) 093103.
[16] S.P. Sullivan, L.F. Gladden, M.L. Johns, L.F. Gladden, Verification of shear-thinning LB simulations in complex geometries, J. Non-Newtonian Fluid Mech. 143 (2007) 59.
[17] C.H. Wang, J.R. Ho, Lattice Boltzmann modeling of Bingham plastics, Physica A 387 (2008) 4740.
[18] A. Vikhansky, Lattice-Boltzmann method for yield-stress liquids, J. Non-Newtonian Fluid Mech. 155 (2008).
[19] G.H. Tang, X.F. Li, Y.L. He, W.Q. Tao, Electroosmotic flow of non-Newtonian fluid in microchannels, J. Non-Newtonian Fluid Mech. 157 (2009) 133.
[20] G.H. Tang, P.X. Ye, W.Q. Tao, Electroviscous effect on non-Newtonian fluid flow in microchannels, J. Non-Newtonian Fluid Mech. 165 (2010) 435.
[21] X.Y. He, L.S. Luo, Lattice Boltzmann model for the incompressible Navier–Stokes equation, J. Stat. Phys. 88 (1997) 927.
[22] T.C. Papanastasiou, Flows of materials with yield, J. Rheol. 31 (1987) 385.
[23] R.B. Bird, G.C. Dai, B.J. Yarusso, The rheology and flow of viscoplastic materials, Rev. Chem. Eng. 1 (1983) 1.
[24] A.N. Alexandrou, T.M. McGilvreay, G. Burgos, Steady Herschel–Bulkley fluid flow in three dimensional expansions, J. Non-Newtonian Fluid Mech. 100 (2001) 77.
[25] Q. Zou, X.Y. He, On pressure and velocity boundary conditions for the lattice Boltzmann BGK model, Phys. Fluids 9 (1997) 1591.
[26] R.B. Bird, W.E. Stewart, E.N. Lightfoot, Transport Phenomena, John Wiley and Sons, New York, 1960.
[27] M.R. Stukan, E.S. Boek, J.T. Padding, W.J. Brielsb, J.P. Crawshaw, Flow of worm-like micelles in an expansion-contraction geometry, Soft Matter 4 (2008) 870.